Extreme Mechanics Letters 1 (2014) 62–69

Contents lists available at ScienceDirect

Extreme Mechanics Letters

journal homepage: www.elsevier.com/locate/eml

Micro-pillar measurements of plasticity in confined Cu thin films

Yang Mu [a], J.W. Hutchinson [b], W.J. Meng [a,*]

[a] Department of Mechanical and Industrial Engineering, Louisiana State University, Baton Rouge, LA 70803, United States

[b] School of Engineering and Applied Sciences, Harvard University, Cambridge, MA 02138, United States

ARTICLE INFO

Article history:
Received 16 October 2014
Received in revised form 23 November 2014
Accepted 3 December 2014
Available online 3 December 2014

Keywords:
Plasticity in confined geometries
Micro-pillar testing protocol
Size effects in plasticity

ABSTRACT

Sputtering was utilized to deposit polycrystalline Cu and CrN films sequentially onto Si(100) substrates, forming specimen assemblies in which predominantly ⟨111⟩ oriented Cu thin films of varying thicknesses were confined between Si and CrN. Cylindrical micro-pillars of CrN/Cu/Si(100) were fabricated through focused ion beam milling, with the interfaces either normal to the axial direction or at an inclination of 45°. Axial compression loading of the micro-pillars produced extensive plasticity within the thin Cu interlayers in both cases, but with distinctly different responses involving combined compression and shear when the interfaces are normal to the compression axis and constrained shear when the interfaces are inclined. Significant size effects were observed, offering new experimental evidence of scale-dependent plasticity for thin film layers, and new experimental test cases for non-local plasticity theories.

1. Introduction

In the last two decades, the dominant experimental means for affecting plastic flow in small volumes, including in thin metal films, has been instrumented micro- and nano-indentation. A methodology for extracting hardness values from experimentally obtained load–displacement curves has been established and well accepted [1]. In particular, a principal avenue through which length scale dependent plasticity effects are demonstrated experimentally has been through the indentation size effect [2]. However, for measuring plastic flow in thin films, substrate influence complicates the determination of the mechanical flow strength using indentation [3,4].

We recently demonstrated a new experimental protocol for evaluating the mechanical integrity of interfaces between hard coatings and substrates [5]. Vapor deposited specimens in the configuration of coating/interlayer/substrate were fabricated via scripted focused ion beam (FIB) milling into microscale cylindrical pillars, with interfaces at a pre-determined inclination angle with respect to the pillar axis. Axial compression loading of the pillars then resulted in interfacial failures, providing a quantitative measurement of the critical failure stress [5]. When the coating and the substrate are both elastic–brittle materials, such as CrN and Si, and the interlayer is a metal, such as Cu, axial compression of micro-pillars with inclined interfaces results in a combination of compressive and shear stress acting on the interlayer. Furthermore, with well bonded interfaces, extensive plastic shearing of thin polycrystalline Cu interlayers was observed, together with a significant dependence of the shear flow stress on the Cu thickness [6].

Shearing of a metal layer bonded between two non-deforming substrates is the iconic example that illustrates the connection between gradients of plastic strain and enhanced flow strength. Due to its analytical simplicity, the confined shear problem has been widely considered as an example in the development of continuum strain gradient plasticity (SGP) and discrete dislocation plasticity (DDP) theories [7–11]. Normal compression of a finite width metal layer bonded between rigid platens has also

* Corresponding author.
E-mail address: wmeng1@lsu.edu (W.J. Meng).

http://dx.doi.org/10.1016/j.eml.2014.12.001

been considered as an application of SGP theories [12]. Normal compression of a metal thin film bonded to platens was suggested as a useful loading geometry for measuring the material length parameter underlying the size effect, especially if companion shear data are available [12]. The micro-pillar experimental technique described in [5,6] creates such a possibility of conducting normal compression and shear tests on the same metal thin film.

In this letter, we report results of axial compression testing on CrN/Cu/Si(100) micro-pillars, with interfaces either perpendicular to the pillar axial direction or at a 45° inclination. Compression testing of the micro-pillars has been performed on an instrumented nanoindenter with a flat punch at different pillar diameters, *D*, Cu interlayer thicknesses, *h*, and over a range of indenter displacements, *d*.

2. Experimental method

Sequential deposition of Cu and CrN onto 50 mm diameter Si(100) wafers was carried out in a custom designed and constructed ultra-high-vacuum vapor deposition tool, which housed a 13.56 MHz inductively coupled plasma (ICP) and four balanced magnetron sputter guns in a load-locked configuration [13–15]. Compositional, structural, and morphological characterizations of deposited thin film specimens were accomplished through X-ray photoelectron spectroscopy (XPS), X-ray diffraction (XRD), transmission electron microscopy and scanning electron microscopy. Electron- or ion-induced secondary electron (SE/ISE) imaging was carried out on an FEI Quanta3D FEG dual-beam FIB instrument with an X-ray energy dispersive spectroscopy (EDS) attachment. The FIB instrument was also used for focused Ga^+ ion milling. XPS data obtained from Cu thin films deposited by ICP assisted sputtering in pure Ar showed no O1s and C1s signals above the background, indicating that oxygen and carbon contaminations within the Cu film were below the instrumental detection limit of ∼1 at.%. XPS data obtained from CrN thin films deposited by ICP assisted reactive sputtering in Ar/N_2 again showed oxygen and carbon contaminations within the CrN layers to be <1 at.%. XPS data obtained from CrN thin films further showed a N:Cr ratio of ∼49:51, close to stoichiometric CrN. XRD data obtained in the θ–2θ geometry showed that sputtered Cu thin films had a strong fiber texture with a predominant orientation of Cu⟨111⟩//Si[100]. The CrN thin films were polycrystalline, with CrN⟨111⟩ and CrN⟨200⟩ being the dominant crystallographic directions parallel to Si[100]. The polycrystalline Cu layers consisted of a random mixture of close to equi-axed Cu grains and columnar Cu grains. The equi-axed grains were ∼20 nm or larger in size. The columnar grains had widths of ∼20 nm or higher, and lengths which can be in the 100–200 nm range. Columnar Cu grains of longer lengths were present in Cu layers of larger thicknesses. The presence of twins was observed, mainly within the columnar Cu grains. There does not appear to be a significant and systematic variation of grain size as a function of the Cu layer thickness. A more detailed statement regarding twin size, spacing, and their dependence on Cu layer thickness requires additional data.

Table 1
A summary of CrN/Cu/Si(100) micro-pillars fabricated and compression tested, with different pillar diameters, *D*, Cu film thicknesses, *h*, and interface inclinations.

Cu interlayer thickness (nm)	CrN/Cu/Si(100) micro-pillar diameter (μm)	
	Interface inclination = 45°	Interface inclination = 0°
∼150	∼4.8	N/A
∼340	∼4.8	N/A
∼550	∼2.8, ∼4.0, ∼4.9	∼5.0
∼810	∼4.6	∼5.0
∼1180	∼4.9	∼3.0, ∼3.9, ∼5.0

Two groups of CrN/Cu/Si micro-pillar specimens were made after cutting each as-deposited wafer into smaller sized pieces. Thin stainless steel sheets of matching sizes were prepared. One micro-pillar group was made by gluing a steel–wafer–steel sandwich assembly, mounting the assembly into epoxy with a fixture which maintained the wafer at a 45° inclination to the epoxy top surface, and polishing the epoxy top surface with SiC abrasives and a final 1 μm diamond suspension to expose the CrN/Cu/Si interfaces [5,6]. The other micro-pillar group was made by directly mounting small Si wafer pieces onto a flat platen, keeping the exposed CrN surface parallel to the platen surface. Scripted Ga^+ milling was used to fabricate micro-pillars perpendicular to the polished surface or the Si wafer surface for cases where interfaces were 45° inclined or perpendicular to the pillar axis. An array of micro-pillars was fabricated for each specimen group. Additional details of the FIB milling process were reported previously [5,6]. The milling process yielded right circular cylindrical pillars with smooth sidewalls and no obvious taper (see e.g., images shown in Fig. 1). In each micro-pillar group, pillars of different diameters were fabricated for one particular Cu interlayer thickness. Table 1 summarizes the combinations of pillar diameters and film thicknesses fabricated and tested.

Compression loading of CrN/Cu/Si micro-pillars was carried out on a NanoIndenter XP with a custom-made, ∼10 μm × ∼10 μm, flat-ended diamond punch. An increasing load was applied to the pillar top surface in displacement-control, with raw indenter load *L* and total indenter displacement *d* monitored continuously. A preset constant loading time was applied to the micro-pillar group with 45° inclined interfaces. A constant loading rate of 10 nm/s was applied to the micro-pillar group with interfaces perpendicular to the pillar axis. A preset *d* value was specified, and the loading was stopped when the specified *d* was reached, followed by load removal. No obvious changes in *L*–*d* curves were observed if loading time or rate were changed. In what follows, raw *L*–*d* curves are presented without correcting for system stiffness contributions.

3. Experimental results

3.1. Confined shear flow stress obtained from micro-pillars with 45°-inclined CrN/Cu/Si interfaces

When the CrN/Cu/Si micro-pillars with 45°-inclined interfaces are loaded in compression, the Cu interlayer experiences a combination of a normal compressive stress

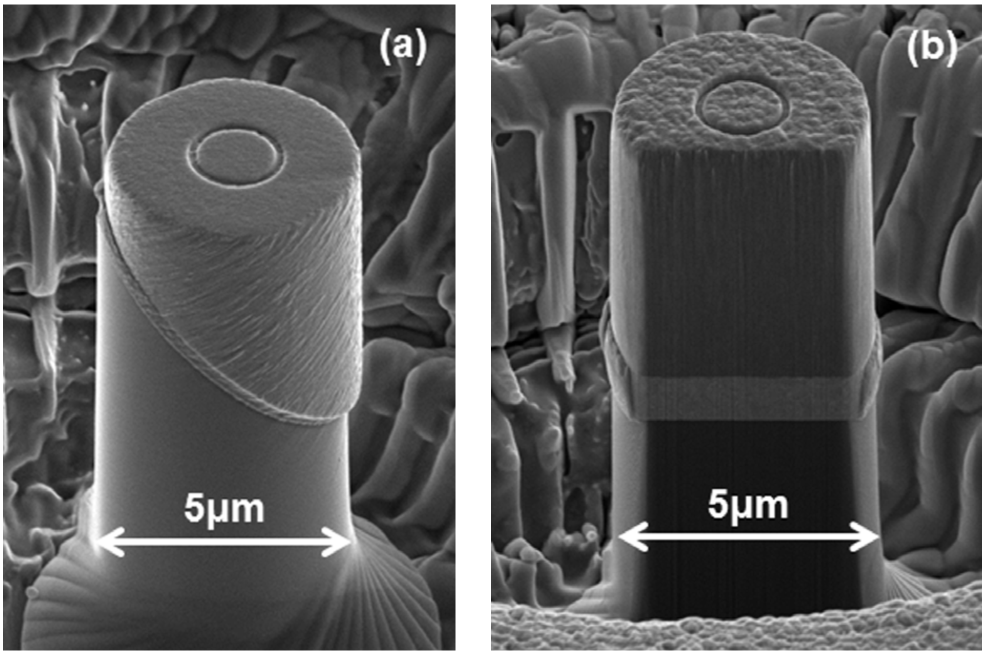

Fig. 1. Examples of the two groups of CrN/Cu/Si micro-pillars following plastic deformation of the Cu interlayer: (a) with the Cu layer inclined at 45° to the compression axis; (b) with the Cu layer perpendicular to the compression axis. In (b), a vertical FIB cut has been made following the deformation to reveal the interfaces and the barreled shape of the material squeezed out at the edge of the layer. Thicknesses of the Cu interlayers in (a) and (b) are ∼340 nm and ∼1180 nm, respectively.

and a shear stress tangent to the layer. When the layer undergoes plastic shearing, the compressive stress normal to the layer is supported by a hydrostatic pressure component which develops within the interior of the layer away from the edges. Because hydrostatic pressure has very little effect on plastic yielding, the micro-pillar compression test is effectively a shear test of the interlayer, consistent with the deformed configuration seen in Fig. 1(a) and further described in Ref. [6]. The average shear stress in the layer is $\bar{\tau} = \bar{\sigma}/2$ with $\bar{\sigma} = L/(\pi D^2/4)$ as the average compressive stress applied to the pillar. For Cu interlayers with thickness $h = 550$ nm, the shear test data are shown in Figs. 2(a) and (b) at three different pillar diameters D, and convincingly demonstrate that D is not a significant factor in determining the average shear flow stress $\bar{\tau}$ of the Cu interlayer. Relatively little hardening occurs after the onset of plastic flow, and $\bar{\tau}$ in Fig. 2(b) is calculated from raw L–d curves based on the plateau load value shown in Fig. 2(a). When L is increasing, deformation of each of the three segments of the pillar contributes to the indenter displacement d. However, when L is on the plateau with the average stress nearly constant, changes in d are due entirely to deformation within the Cu interlayer because the Si and CrN segments remain elastic.

While D has essentially no influence on $\bar{\tau}$, the layer thickness h has a large influence, as shown in Fig. 2(c), with a factor of two difference in the average shear flow stress observed over the h range tested (150–1180 nm). As will be discussed later, in connection with the predictions from the SGP theory in Fig. 2(c), an essential aspect of this behavior is the fact that dislocation motion in Cu is blocked at the CrN/Cu and Cu/Si interfaces, thus constraining the plastic flow. Note also that several tests have been conducted for each combination of D and h, with low scatter in measured $\bar{\tau}$ values. To our knowledge, the experimental data reported in Fig. 2 is the first set to become available for confined shearing of layers with thicknesses in the nanometer to micron range. An earlier effort using a different experimental approach was not fully successful [16]. Further aspects of the shear tests are discussed in [6].

3.2. Average compressive flow stress obtained from micro-pillars with CrN/Cu/Si interfaces perpendicular to the compression axis

In this case, a Cu interlayer, well bonded to the adjoining elastic sections of the pillar, is only able to deform plastically by undergoing a combination of compressive plastic straining in the axial direction and shearing that allows the metal to be squeezed out at the perimeter of the layer. The shear is zero at the axis of symmetry and increases with distance from that axis. Moreover, while shear in the Cu layer oriented at a 45° inclination to the micro-pillar axis occurs in one direction throughout the thickness, shear in the perpendicularly oriented Cu layer has one sign above the layer mid-plane and the opposite sign below the mid-plane. Gradients of plastic strain in this configuration occur in both the radial and through-thickness directions such that the dependence of plastic flow on the material length parameter is expected to be unusually strong. The CrN/Cu and Cu/Si interfaces again block dislocation motion and constrain plastic straining at the interfaces. Visual evidence of this constraint can be seen in Fig. 1(b) where barreling is seen at the perimeter of the Cu interlayer. Had the Cu been able to flow plastically at the interfaces, a step in the Cu layer at each of the interfaces would be observed.

Raw L–d curves for Cu layers with thickness of 1180 nm are shown in Fig. 3(a) for three different D values. An intermediate plateau in the load versus indenter displacement

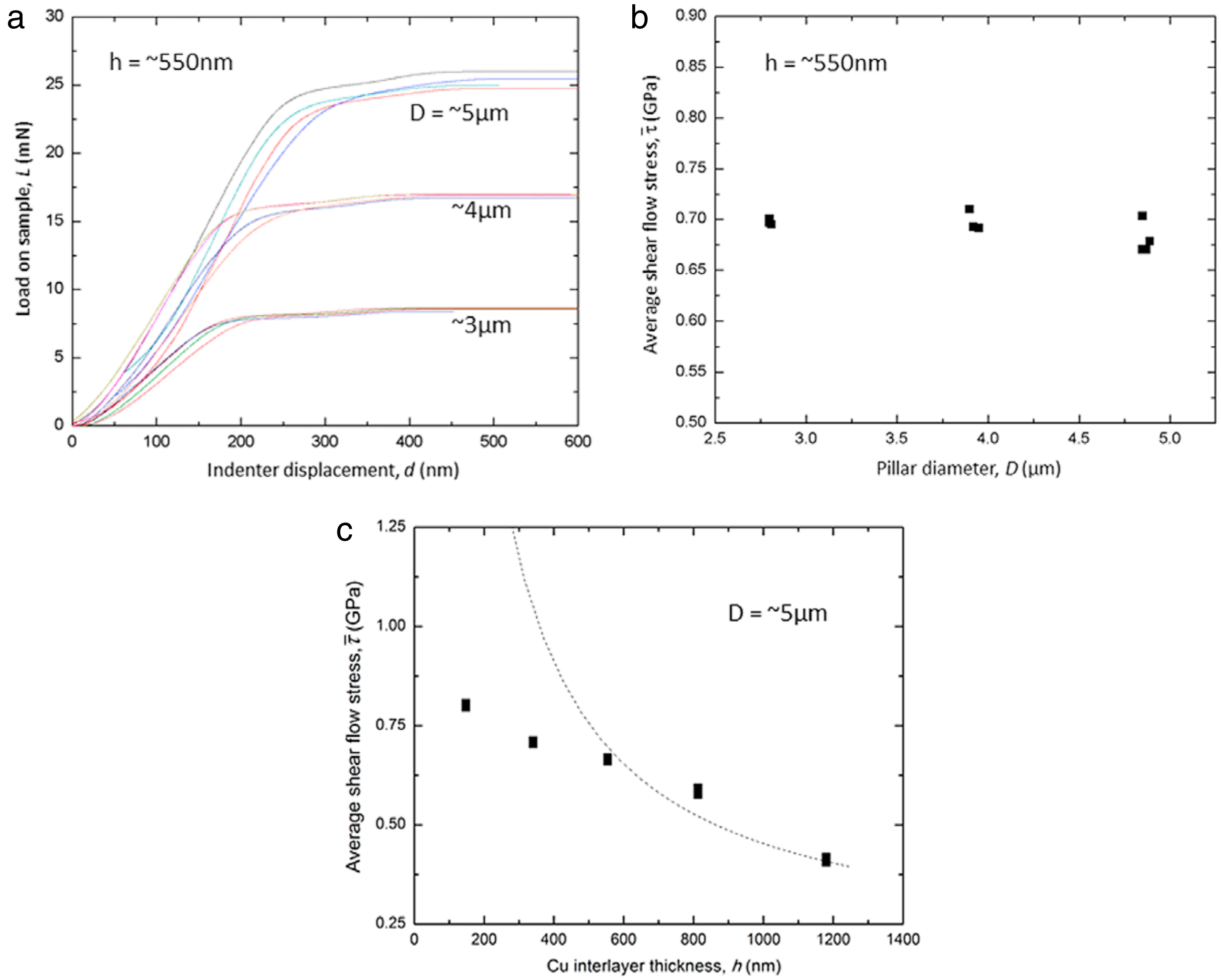

Fig. 2. Confined shear data obtained from CrN/Cu/Si micro-pillars with interfaces inclined at 45° to the compression axis: (a) Raw load L versus indenter displacement d for three pillar diameters, D, with Cu interlayer thickness, $h = \sim 550$ nm. (b) Average shear flow stress based on load plateau of the data in (a), revealing that D has almost no influence on the shear flow stress. (c) Average shear flow stress versus h, obtained from pillar specimens having $D = \sim 5$ μm. The strong dependence of the shear flow stress on h is revealed by (c). Multiple tests have been conducted for each combination of h and D, with relatively little scatter evident in the data. The dashed line in (c) shows output from the SGP model.

is followed by a steadily increasing load. The average compressive flow stress $\bar{\sigma}$, shown in Fig. 3(b), is evaluated using the load on the plateau. We do not fully understand the reason for the transition from the load plateau to a further increasing load. The indenter displacement change associated with the plateau in Fig. 3(a) ranges from $\sim$200 to $\sim$500 nm and, for the layer with thickness of 1180 nm, this constitutes a significant change in thickness. Associated with this large thickness change are even larger shear strains near the perimeter of the layer. Plastic strains of 30% or larger occur throughout the layer on the plateau, dominating the elastic strains. It is possible that the transition from the load plateau to a further increasing load is due to aspects of finite deformation, including the formation of the collar ring at the outer edge of the layer, but further studies are necessary to reach a definitive conclusion.

Fig. 3(b) reveals the strong influence of the pillar diameter, D, on the average compressive flow stress for a fixed h. An increasing $\bar{\sigma}$ would be expected even from conventionally plasticity [17], however the presently observed dependence of $\bar{\sigma}$ on D is stronger than what would be expected without a material size effect, as discussed in the next section. Fig. 3(c) shows that, for a fixed D, $\bar{\sigma}$ exhibits an even stronger dependence on the Cu layer thickness h, increasing by a factor of two as h decreases from 1180 to 550 nm. Similarly, this dependence of $\bar{\sigma}$ on h is much too strong to be explained without a material size effect.

4. The material length parameter and trends predicted by strain gradient plasticity

The purpose of this section is to illustrate that the experimental trends shown in Figs. 2 and 3 are qualitatively captured by predictions of an elementary SGP model with one consistent set of material parameters. Subsequent efforts will be made to obtain more accurate agreement with the experimental results. Indeed, in part, the value of the present set of experimental data is that it can serve as a test case for the further development of SGP and DDP—theories which are not yet sufficiently reliable for applications purposes.

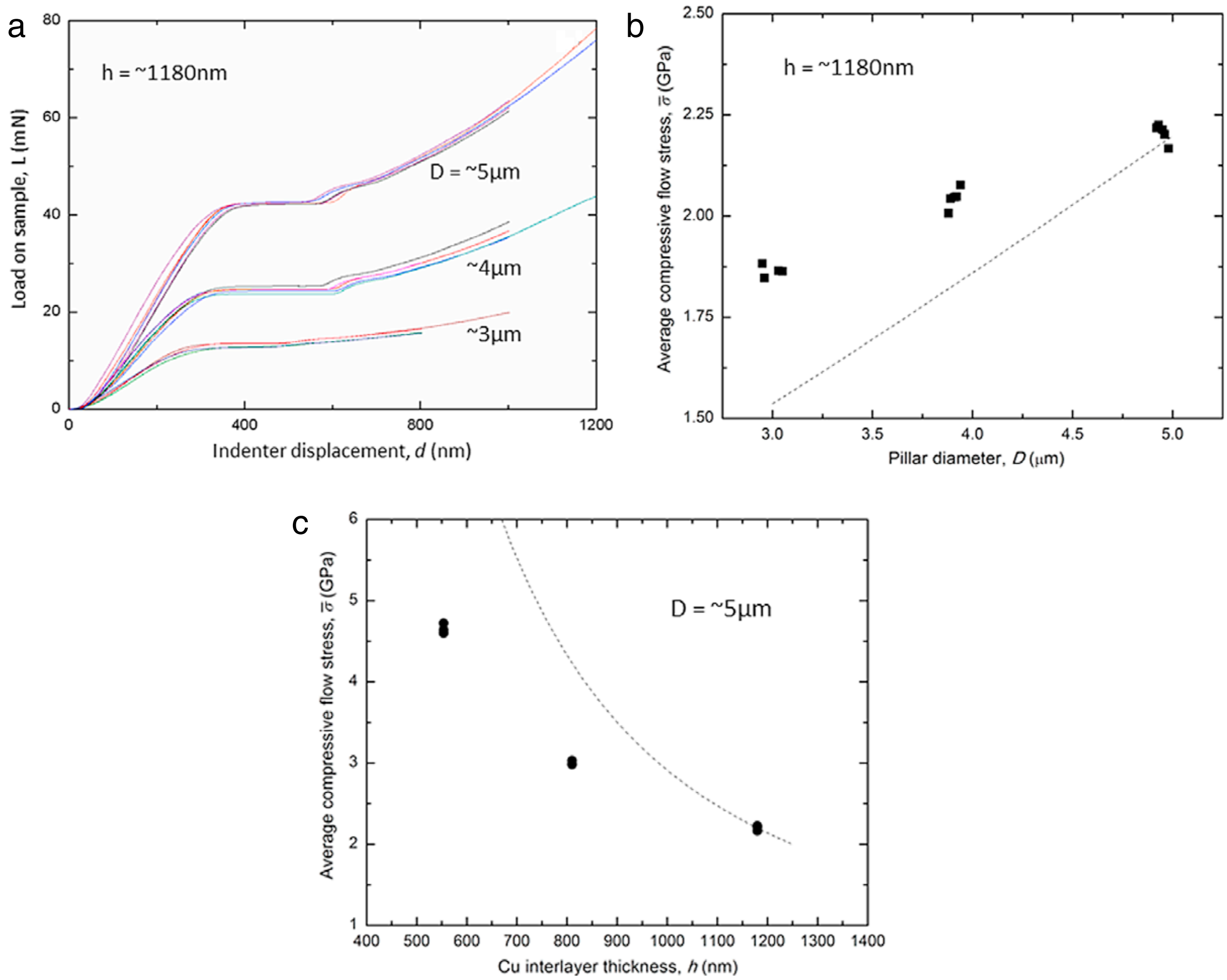

Fig. 3. Normal compression data obtained from CrN/Cu/Si micro-pillars with interfaces oriented perpendicular to the compression axis: (a) Raw load L versus indenter displacement d for three pillar diameters, D, with Cu interlayer thickness $h = \sim 1180$ nm. (b) Average compressive flow stress versus D based on intermediate load plateau of the data in (a). (c) Average compressive flow stress versus h, obtained from pillar specimens having $D = \sim 5$ µm. In normal compression, a factor of two decrease in h produces more than a factor of two increase in the compressive flow stress. Multiple tests have been conducted for each combination of h and D, with relatively little scatter evident in the data. Dashed lines in (b) and (c) show outputs from the SGP model.

A simple small strain deformation theory of SGP [7,12] will be employed here, which has three material parameters: a reference flow stress, σ_Y, a strain hardening exponent, N, and a material length parameter, l. The uniaxial tensile stress–strain relation is assumed to follow the power law: $\sigma = \sigma_Y \varepsilon^N$. An effective plastic strain is defined as $E_P = \sqrt{2\varepsilon^P_{ij}\varepsilon^P_{ij}/3 + l^2 2\varepsilon^P_{ij,k}\varepsilon^P_{ij,k}/3}$, which combines the conventional effective plastic strain with an analogous term formed from the plastic strain gradients and the material length parameter. Elastic strains are neglected, and the work density under proportional straining is $U(E_P) = [\sigma_Y/(N+1)]E_P^{N+1}$. In the deformation theory, this work density is identified with the strain energy density of the solid. It reproduces $\sigma = \sigma_Y \varepsilon^N$ in uniaxial tension. The energy in the layer is $\Phi = \int_V U(E_P)dV$ where V is the layer volume. At a prescribed average shear strain across the layer in the shear case, or at a prescribed uniform normal relative displacement of the interfaces in the normal compression case, the desired strain distribution minimizes Φ among all admissible distributions. Admissibility requires that the plastic strains vanish at the interfaces with the adjoining segments of the pillar, modeling the blocked dislocation motion.

The raw L–d curves, shown in Figs. 2(a) and 3(a), indicate that within the flat plateau region there is relatively little strain hardening. Thus, the predictions which follow will be based on the limit $N \to 0$, such that the solid is rigid-perfectly plastic and characterized by the tensile yield stress σ_Y and material length parameter l. The computations for the normal compression case have been carried using a method similar to that detailed in Ref. [12], but for the present axisymmetric geometry rather than plane strain. Predictions from the model are presented in dimensionless form in Fig. 4, covering the parameter variations of the experiments discussed in Section 3. The strong dependence on h/l in each part of Fig. 4 highlights the influence of the material length parameter. The predictions asymptote to those for a conventional rigid-perfectly plastic solid when $h/l > 5$. The predicted response of an rigid-perfectly plastic solid without strain gradient effects, i.e., the limit as $l/h \to 0$, is also included in Fig. 4 for comparison.

To make a direct comparison with the experimental results shown in Figs. 2 and 3, it is necessary to assign

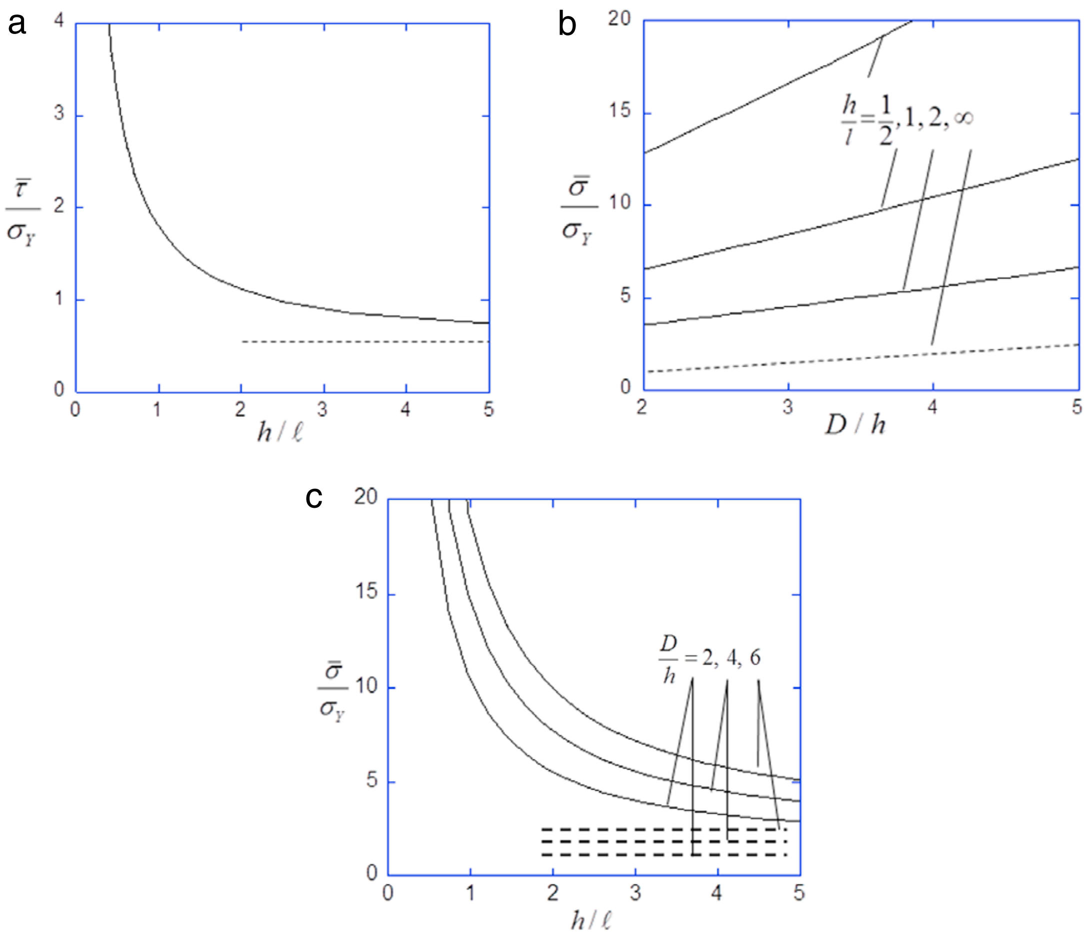

Fig. 4. Trends predicated by the simple strain gradient plasticity model (solid lines) described in the text for a solid in the perfectly-plastic limit having a tensile (and compressive) flow stress σ_Y and a material length parameter l: For the layer in confined shear, (a) shows the average shear flow stress normalized by σ_Y versus the ratio of h to l; For the layer in normal compression, the average compressive flow stress normalized by σ_Y is shown in (b) versus the ratio of D to h, and in (c) versus the ratio of h to l. The dashed lines denote model output without strain gradient effects.

values to σ_Y and l. We have not made independent measurements of tensile yield stress of Cu thin films, but several papers on this subject exist in the literature [18]. Reported σ_Y values are in the range of 0.3–0.4 GPa for Cu thin films of thicknesses around 1 μm or larger. In the following simulations, we take $\sigma_Y = 0.35$ GPa. Then, based on the SGP results shown in Fig. 4(a), we choose l to reproduce the experimentally measured average shear flow stress, $\bar{\tau} = 0.70$ GPa, in Fig. 2(b) for Cu layers with $h = 550$ nm, yielding an l value of 647 nm. It is interesting to note that previous tensile testing of supported Cu thin films [19] and bulge testing of free-standing Cu thin films [20] with surface passivation yielded respectively l values of ∼0.6 μm and ∼0.35 μm, largely consistent with the present fitted l value.

The SGP model predictions, computed with the single parameter set of $\sigma_Y = 0.35$ GPa and $l = 647$ nm, are plotted in dimensional form as dashed lines in Figs. 2(c), 3(b), and 3(c). As evident from these figures, while the predictions of the simple SGP theory capture the general trend in each of the three comparisons, they overestimate the strength enhancement for the thinner layers. In addition, the theory predicts a stronger increase in $\bar{\sigma}$ with pillar diameter than what is observed in the experimental data. As noted above, the present SGP model is the simplest theory one could choose. One obvious limitation which is likely to be important is the fact that the model is isotropic and thereby ignores plastic anisotropy associated with the dominant ⟨111⟩ fiber texture of the Cu grains. More accurate predictions may require a single crystal representation of the polycrystalline layer. This and other possibilities are left for the future. We also note that the present set of polycrystalline Cu interlayers, at any thickness studied, contain numerous grain boundaries which can serve as dislocation sources. In addition, all Cu interlayers were deformed to large plastic strains as a result of the loading applied. The present data should serve as a challenge for both continuum and DDP theories.

5. Concluding remarks

A new experimental protocol has been described for testing plasticity of thin metal films confined between and bonded to non-deforming, elastic–brittle materials in a micro-pillar geometry. Experimental results for plastic flow of sputtered Cu thin films in both confined shear and normal compression have been obtained from CrN/Cu/Si micro-pillars. These results have been compared to a simple strain gradient plasticity model for a perfectly plastic solid characterized by an unconstrained tensile yield stress $\sigma_Y = 0.35$ GPa, which was identified using data for free standing films from the literature, and a material length parameter $\ell = 647$ nm, which was chosen to fit the present shear data for Cu film with a thickness of 550 nm. The Cu film thicknesses tested (550–1180 nm) encompass the material length parameter, and the testing results reveal a factor of two increase of the effective shear strength of the thinnest film relative to the thickest film. Furthermore, the effective shear strength of the thickest confined Cu film (1180 nm) is already twice that expected for the Cu shear strength under unconfined conditions, i.e., 0.4 GPa compared with $\sigma_Y/\sqrt{3} = 0.2$ GPa. Thus, the experimental data obtained for the thinnest Cu films (550 nm) for both the shear test and the normal compression test reveals an elevation of the effective strength of the Cu by a factor of four above the value expected for thicker films—a significant size effect. The simple SGP model captures the essential trends of Cu film deformation in both confined shear and normal compression geometries, but improvements in quantitative agreement with experimental data will require further modeling efforts.

Until now, plasticity in metal thin films has been experimentally probed by instrumented nanoindentation and tensile testing of either free-standing metal films or metal films supported on polymeric substrates. While substrate effects complicate indentation testing of thin films on substrates, the experimental complexity associated with tensile testing of free-standing or supported thin films curtails its wide usage. In comparison, the present experimental results illustrate that extensive plastic deformation can be induced within thin metal films by using the micro-pillar protocol described in this letter, and that this protocol allows quantitative plasticity data to be obtained from the same metal film under significantly different deformation geometries. The new experimental results presented in this letter offer independent test cases for confronting new developments in SGP—the wide range of parameters capable of being represented in such data sets is believed to be valuable for further experimental calibration and validation of non-local plasticity theories.

In addition to the scientific interest in understanding micro- and nano-scale mechanical behavior of materials, plastic flow in confined thin metal layers is also of significant interest to surface engineering technologies. Vapor phase deposition of thin ceramic coatings has become an important means for engineering surfaces of mechanical components [21,22] and manufacturing tools [23,24]. Satisfactory adhesion of coatings to substrates is critical to the lifetime of coated systems. To improve adhesion between ceramic coatings and substrates, thin metallic interlayers are often deposited between the coating and the substrate. When coated components are subjected to external contact, this adhesion interlayer is put under combinations of compression and shear. How such thin interlayers deform plastically has a significant bearing on the mechanical response of the coating/interlayer/substrate system as a whole. Data presented here represent, to our knowledge, the first set of quantitative data on how thickness and deformation geometry of thin metal interlayers influence their plastic behavior under stress conditions relevant to interlayer performance. It is hoped that further investigations along the lines outlined in this letter will advance the fundamental understanding on how to effectively engineer coating/substrate interfaces for wide ranging applications of coated mechanical components and manufacturing tools.

Acknowledgments

Partial project supports for YM and WJM from National Science Foundation and LA BoR through grant CMMI-0900167 and contract LEQSF(2013-16)-RD-B-01 are gratefully acknowledged. JWH acknowledges interactions with C.F. Niordson and the grant "Higher order theories in solid mechanics" of the Danish Council for Independent Research, grant 11-105098/FTP.

References

[1] W.C. Oliver, G.M. Pharr, An improved technique for determining hardness and elastic modulus using load and displacement sensing indentation experiments, J. Mater. Res. 7 (1992) 1564–1583.
[2] Q. Ma, D.R. Clarke, Size dependent hardness of silver single crystals, J. Mater. Res. 10 (1995) 853–863.
[3] T.Y. Tsui, G.M. Pharr, Substrate effects on nanoindentation mechanical property measurement of soft films on hard substrates, J. Mater. Res. 14 (1999) 292–301.
[4] R. Saha, W.D. Nix, Effects of the substrate on the determination of thin film mechanical properties by nanoindentation, Acta Mater. 50 (2002) 23–38.
[5] K. Chen, Y. Mu, W.J. Meng, A new experimental approach for evaluating the mechanical integrity of interfaces between hard coatings and substrates, MRS Commun. 4 (2014) 19–23.
[6] Y. Mu, K. Chen, W.J. Meng, Thickness dependence of flow stress of Cu thin films in confined shear plastic flow, MRS Commun. 4 (2014) 129–133.
[7] N.A. Fleck, J.W. Hutchinson, Strain gradient plasticity, Adv. Appl. Mech. 33 (1997) 295–361.
[8] J.Y. Shu, N.A. Fleck, E.Van der Giessen, A. Needleman, Boundary layers in constrained plastic flow: comparison of nonlocal and discrete dislocation plasticity, J. Mech. Phys. Solids 49 (2001) 1361–1395.
[9] E. Bittencourt, A. Needleman, M.E. Gurtin, E.Van der Giessen, A comparison of nonlocal continuum and discrete dislocation plasticity predictions, J. Mech. Phys. Solids 51 (2) (2003) 281–310.
[10] P. Fredriksson, P. Gudmundson, Size-dependent yield strength of thin films, Int. J. Plast. 21 (9) (2005) 1834–1854.
[11] S.P. Lele, L. Anand, A small-deformation strain-gradient theory for isotropic viscoplastic materials, Phil. Mag. 88 (30–32) (2008) 3655–3689.
[12] C.F. Niordson, J.W. Hutchinson, Basic strain gradient plasticity theories with application to constrained film deformation, J. Mech. Mater. Struct. 6 (2011) 395–416.
[13] W.J. Meng, T.J. Curtis, Inductively coupled plasma assisted physical vapor deposition of titanium nitride coatings, J. Electron. Mater. 26 (1997) 1297–1302.
[14] W.J. Meng, T.J. Curtis, L.E. Rehn, P.M. Baldo, Temperature dependence of inductively coupled plasma assisted deposition of titanium nitride coatings, Surf. Coat. Technol. 120–121 (1999) 206–212.
[15] W.J. Meng, E.I. Meletis, L.E. Rehn, P.M. Baldo, Inductively-coupled plasma assisted deposition and mechanical properties of metal-free and Ti-containing hydrocarbon coatings, J. Appl. Phys. 87 (2000) 2840.
[16] V.L. Tagarielli, N.A. Fleck, The shear response of a thin aluminum layer, J. Appl. Mech. 78 (2011) 014505/1-3.
[17] R. Hill, The Mathematical Theory of Plasticity, Oxford University Press, New York, 1998.
[18] H. Huang, F. Spaepen, Tensile testing of free-standing Cu, Ag and Al thin films and Ag/Cu multilayers, Acta Mater. 48 (2000) 3261–3269.
[19] D.Y.W. Yu, F. Spaepen, The yield strength of thin copper films on Kapton, J. Appl. Phys. 95 (2004) 2991–2997.
[20] Y. Xiang, J.J. Vlassak, Bauschinger and size effects in thin-film plasticity, Acta Mater. 54 (2006) 5449–5460.

[21] J.C. Jiang, W.J. Meng, A.G. Evans, C.V. Cooper, Structure and mechanics of W-DLC coated spur gears, Surf. Coat. Technol. 176 (2003) 50–56.
[22] M. Eckels, M.N. Kotzalas, G.L. Doll, Attaining high levels of bearing performance with a nanocomposite diamond-like carbon coating, Tribol. Trans. 56 (2013) 410–416.
[23] S. PalDey, S.C. Deevi, Single layer and multilayer wear resistant coatings of (Ti, Al)N: a review, Mater. Sci. Eng. A 342 (2003) 58–79.
[24] D.M. Cao, W.J. Meng, Microscale compression molding of Al with surface engineered LiGA inserts, Microsyst. Technol. 10 (2004) 662–670.